

# Prediction of Residual Stresses and Springback in Multi-pass Sheet Metal Spinning Using Finite Element Analysis

Mohamed Abd-Alrazzaq<sup>1</sup> • Mahmoud Hamed Ahmed<sup>1</sup> • Mohammad A. Younes<sup>1\*</sup>

**Abstract**— In the recent decades, multi-pass sheet metal spinning proved to be a critical process for many industrial components such as jet engines, large size pressurized tanks and vessels, but residual stresses and springback in these spun parts remain an alarming problem. This study is intended to provide wider insight into the controlling parameters of these features. Two finite element (FE) simulations were conducted based on explicit code for the spinning process and implicit code for springback and residual stresses prediction. The numerical results were verified and found to be well correlated with the experimental data. Optimum combination between small springback and safety against residual stresses was obtained using low feed ratio and friction coefficient with large number of spinning passes. The common issue is low loading rate. Better control of the final spinning pass can add value to the mechanical and dimensional characteristics of the spun component.

**Keywords**— Multi-pass sheet metal spinning, Residual stresses, Springback, Finite element analysis, Pressure vessels

## I. Introduction

Sheet metal spinning has recently become a priority process for high strength to weight ratio components for aerospace and transportation applications [1]. In this process, a sheet blank is clamped between a rotating mandrel and a holder then a roller is moved through a special path to deform the sheet metal into the desired shape in one or multiple passes over the mandrel surface [2, 3]. Lower tooling cost, material saving, and geometrical alterations (cones, cylinders, spheres) are added values in metal spinning besides the benefit of strain hardened walls of the spun body such as tank segments [4].

The residual stresses induced in spun components such as jet engine parts affect both their fatigue life and springback characteristics. The spinning process variables contribute to the distribution and magnitude of the generated pre-service residual stresses [5, 6]. Dierig used hole drilling to measure residual stresses after spinning and observed outer sheet surface tensile values and inner surface compressive values [5]. Using FE conventional spinning simulation, Watson and Long found high residual stresses generated by the roller tool contact leading to bending moments in the blank sheet flange [7]. Zoghi et al. predicted Von Mises residual stresses in dome spinning using FE analysis to be larger as the feed ratio increases [8].

Gür and Arda evaluated the tangential residual stresses on the surface of spun tubes using a slitting technique and found them to be tensile and increasing with the progress of deformation [9]. Zhen and Guo-Yue deduced the residual shear stress in spun aluminum alloy tubes using splits on one side. It was found to be linearly distributed through the wall thickness reaching a maximum at the inner surface [10]. Fuan et al. and Yong et al. reported that higher tensile residual stresses particularly in the circumferential direction are the major parameter that causes cracks in the surface of spun tubes with possibility of metal embrittlement [11, 12]. Residual stresses in spun tubes may result in fish scaling with the aid of non-uniform grain size and inclusions [13]. Šugár et al. used X-ray diffraction method to measure residual stresses on outer surface of cups produced by CNC multi-pass conventional spinning. The geometrical configuration of the spun part was found to be the significant parameter affecting sub-surface residual stresses with minimum values at corner radius of the cup. Planar anisotropy of the raw sheet material has negligible effect on residual stresses [14].

El-Khabeery et al. studied springback in spun aluminum cups and found that higher feed ratio and larger roller tool angle result in inner diameter expansion [15]. Wang and Long found that elastic strain energy rises during the spinning process and a considerable elastic recovery takes place when the roller moves away from the work part at the end of each effective roller pass [16]. Essa and Hartley observed an increasing trend of springback with increasing feed ratio and enlargement in inner diameter at the spun cup open end [1]. Similar findings were achieved by Kawai et al. [17]. Venkateshwarlu et al. noticed that springback in radial direction of the cup opening is lower with higher mandrel rotational speed and is larger as compared to cup bottom [18]. Han et al. provided the fittability quality index associated with springback as the maximum gap size between the spun part and the mandrel. Large ratio of yield stress  $\sigma_0$  to Young's

---

Tel.: +20-1221037855

ORCID iD: 0000-0003-0061-3854

Mohammad Abdelwahed Younes (corresponding author)

<sup>1</sup> Production Engineering Department, Faculty of Engineering, Alexandria University, Alexandria, 21544, Egypt

modulus  $E$  ( $\sigma_0/E$ ) induces higher springback [19]. Wang et al. found proportionality between wall thickness reduction and springback [20].

Roller force in multi-pass spinning process is the driving source of residual stresses and springback in sheet metal parts. It can be resolved in the three perpendicular directions; axial force -  $F_a$  parallel to the axis of the mandrel, radial force -  $F_r$  in line with the radius of the mandrel and tangential force -  $F_t$  to the deformed sheet blank perimeter at the roller contact point [3]. Xia et al. [21] demonstrated that axial force is the largest at the beginning of the spinning process, while the radial force is the highest at the final stage owing to ironing effect. On the other hand, the tangential force is always the smallest remaining relatively constant over the entire process time [22].

FE simulations of sheet metal spinning were developed in 1990s. By the majority of researchers, the explicit FE method was found to be the most effective in the analysis of sheet metal spinning process due to the use of diagonal mass matrices for the accelerations without convergence checks. This is advantageous for complex problems such as nonlinear dynamic and quasi-static metal forming analyses with complicated contact behavior [3, 23–26]. On the other hand, implicit FE method can handle springback and residual stresses simulations more rapidly than explicit FE method owing to gentle nonlinearities and no contact involved so the chosen procedure to simulate springback and residual stress after sheet metal spinning is to transfer the finished spin-forming model from explicit into implicit environment [20, 27–29]. Continuum shell elements; with multiple integration points through the thickness and double-sided contact capability, are preferred in FE meshing for sheet blanks in conventional metal spinning simulations due to the accuracy of force, stress, strain and thickness results compared to 3D solid elements that uses only one integration point in the thickness direction [16, 30,31]. The sweep meshing strategy in conventional spinning simulation provided good correlation between FE and experimental results due to its regularity particularly when the central clamped area is neglected [28, 32]. Both sliding and rolling friction with dynamic complex contact is prevailing between the roller tool and the sheet blank so the penalty contact approach was adopted in conventional sheet spinning simulations and showed reliable performance [29, 33]. The frictional effect causes the roller to rotate around its axis [3]. Accordingly, most researchers such as Essa and Hartley [1], Wang and Long [31], and Liu [33] assumed coulomb coefficient of friction (0.02–0.1) between the roller tool and the sheet blank.

Based on the available literature, limited research regarding residual stresses has focused on conventional spinning processes. Mainly the effect of speed parameters such as feed ratio and mandrel speed was investigated for springback and residual stresses in conventional spinning with no mention of friction coefficient and number of spinning passes as influencing factors. Limited work on the impact of part geometry was found especially the sheet thickness. Severity of circumferential tensile residual stresses should be highlighted as an indicator of possible crack formation. Consequently, the present study is intended to cover these

knowledge gaps and provide more comprehensive insight into the springback and residual stresses behavior of spun parts particularly large size tank and pressure vessel segments under difficult service conditions.

## II. Finite Element Model

A finite element model has been developed for multi-pass sheet metal spinning of cylindrical cups using ABAQUS/CAE 6.13 software. In the spinning process, a circular sheet blank is clamped between a rotary mandrel and a back-plate called holder. Shaping of the sheet is performed gradually over the mandrel via a roller motion on the sheet surface. In this FE model, the mandrel has a cylindrical shape of 190 mm diameter and revolves at a speed of 200 rpm. This low rotational speed is suitable to simulate large size applications. An aluminum circular sheet blank with an original diameter of 240 mm is attached to the mandrel. The holder has a diameter of 124 mm. Figure 1 shows the process geometries and configuration.

At first, the holder compresses the sheet towards the mandrel with a force of 100 kN [34]. The mandrel, sheet, and holder were given tie constraints to make them rotate with the same revolution speed. The roller tool, mandrel and holder are modeled as analytical rigid parts [27, 34]. The sheet blank is modeled as a pure aluminum (A 1050-O) deformable part of 2,700 kg/m<sup>3</sup> density. A 1050-O data are fed to the ABAQUS software as an elastic-plastic material based on uniaxial tension test results of a flat specimen under ASTM E8–04 standard. True stress–true plastic strain diagram (double log-scale) is illustrated in Figure 2 along with the specimen dimensions. The proof stress, Young's modulus and Poisson's ratio are 29 MPa, 70 GPa, and 0.33 respectively.

A dynamic explicit analysis step has been used. The explicit method provides the solution without iteration, just advancement of the kinematic parameters through time increments [35]. It is preferable for the metal spinning process which is a quasi-static forming problem with large plastic deformation and a state of complicated contact [26]. Geometric non-linearity option was activated due to the complex mode shapes of the sheet during deformation. The penalty contact method was used and Coulomb friction coefficient was set to be 0.2 and 0.5 between the sheet blank and the mandrel and holder respectively [34]. The mass inertias of holder and roller tool are established based on the density of the steel material used for them so that they can revolve about their axes when coming in contact with the sheet.

An 8-node reduced integration linear continuum shell elements (SC8R) with enhanced hourglass (element bending behavior) control are used to mesh the sheet to provide accurate FE solutions. Nine integration points have been used in the direction of element thickness to obtain accurate state of stress along the sheet thickness [16,30,31]. The annular zone that contacts the mandrel round corner has more elements to develop smooth contact and improve the bending behavior in this region [34]. Since there is not any deformation, the circular clamped region (59 mm radius) of the sheet under the

holder surface is not meshed and excluded from the analysis. A medial axis sweep mesh technique is used with total number of elements of 2160 and total number of nodes of 4560 as presented in Fig. 3. These numbers of elements and nodes were selected based on a mesh density sensitivity analysis of the first spinning pass for 4 different meshing schemes as stated in Table I.

There is no significant difference between the FE results of the four meshes, so the mesh that yields the minimum processing time is preferable. The simulations were conducted on a workstation of eight cores Intel® Xeon® CPU L5630, 2.13 GHz (2 processors) and 24 GB RAM. Parallelization method was used to reduce the computational time significantly without affecting the accuracy of results [24].

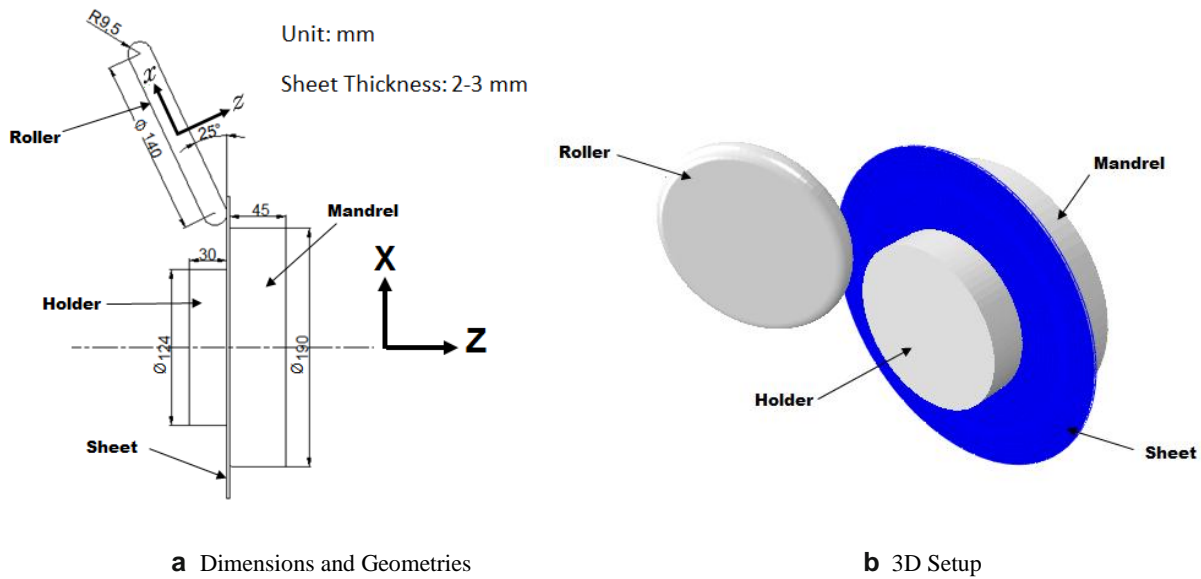


Figure 1. FE model configuration.

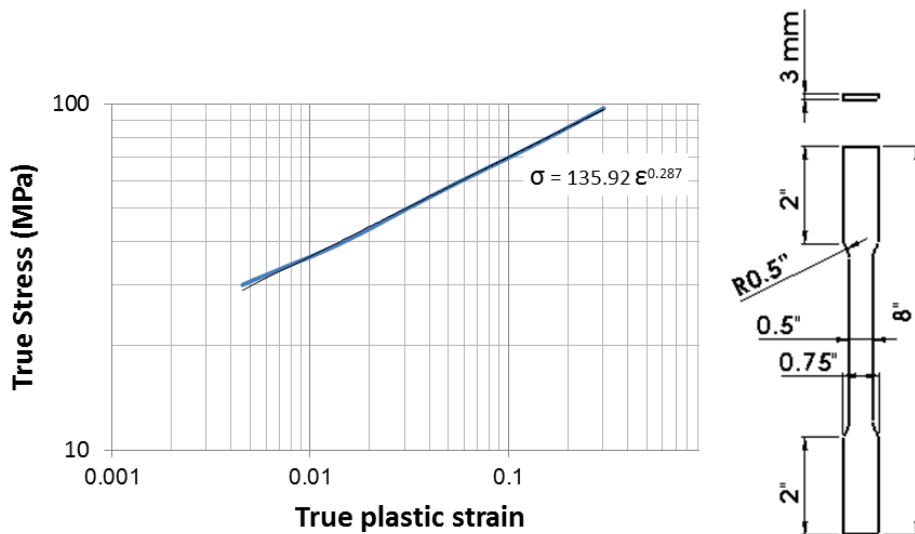


Figure 2. True stress-true plastic strain diagram and tension test specimen.

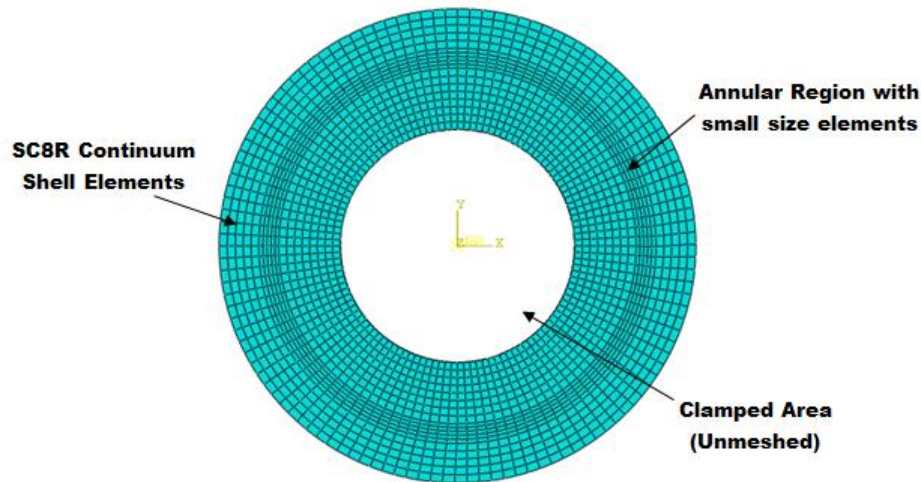


Figure 3. Sheet blank meshing.

TABLE I. MESH DENSITY SENSITIVITY ANALYSIS RESULTS

FE Model	Number of elements	Circumferential nodes	Total number of nodes	Processing time (hr:min:sec)	Axial force (N)	Minimum thickness, mm
1	2160	120	4560	8:50:32	819.834	1.99612
2	2679	140	5640	12:55:17	874.048	1.99759
3	3381	160	7084	15:53:46	808.215	1.99986
4	3982	180	8326	20:20:39	797.992	1.99429

### III. First Numerical Simulation

#### A. Considered Variables

A first FE simulation was performed based on three variables; sheet thickness, feed ratio, and friction coefficient as stated in Table II. The sheet thicknesses were selected based on availability. Feed ratio range provides higher processing speed and productivity especially for large tank segments. Friction coefficients between the roller tool and the sheet surface, cover the common range studied in the available literature [1, 31, 33] and introduce insight for all conditions regarding lubrication; dry condition, average lubrication, and excellent lubrication [36]. All combinations between these variables were considered in the simulations, so the total number of runs is 18. All runs employed 10 successive spinning passes as shown in Fig. 4. The forward passes are involute curves to optimize the process performance in terms of required force, induced stresses and strains, and material defects [5]. Backward linear passes are effective in reducing the redundant processing time because no contact between the roller and the sheet takes place in these stages.

The FE simulations in this study were developed from the process settings of computer numerically controlled (CNC) multi-pass spinning experiments. A retrofitted CNC spinning

machine was operated using the Computer-Aided Manufacturing (CAM) software - Eding CNC Release 4.00.46 to establish the roller tool path in Fig. 4 as a CNC program. In the FE model, the roller is given two displacement boundary conditions in the local  $x$  and  $z$  directions, as illustrated in Fig. 1. The roller tool path coordinates were transferred from the CNC program which is based on the global coordinate system ( $X$ - $Z$ ) to the roller local coordinates ( $x$ - $z$ ). Two equations are adopted to compute the local coordinates directly from the global coordinates [3]:

$$z = Z \cos \theta + X \sin \theta \quad (1)$$

$$x = X \cos \theta - Z \sin \theta \quad (2)$$

The angle  $\theta$  between the roller (local coordinates) and mandrel (global coordinates) axes is  $25^\circ$  as shown in Fig. 1.

TABLE II. CONSIDERED VARIABLES IN FIRST NUMERICAL SIMULATION

Variable	Chosen Values		
Sheet Thickness (mm)	2	3	
Feed Ratio (mm/revolution)	1	2	3
Coefficient of Friction	0.02	0.05	0.1

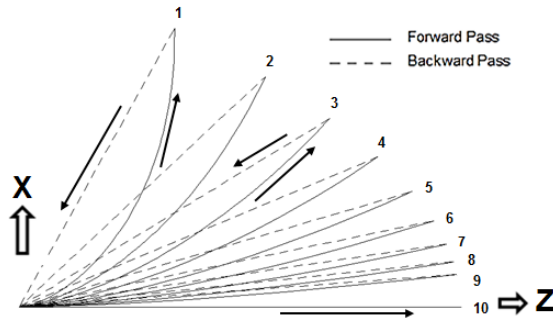


Figure 4. First simulation roller tool path.

As residual stresses and springback analyses are static in nature without applying any external loads or contact conditions, ABAQUS/Implicit can achieve a solution in a small number of increments [35]. The spinning FE simulation results obtained using ABAQUS/Explicit, as mentioned in Section II, were imported to ABAQUS/Implicit to estimate the residual stresses and springback in the spun cups using FE analysis. All external loads and boundary conditions were removed. Mandrel, holder, and roller were released to allow the spun cup to springback freely without any contact interactions. A general static analysis step was defined including the geometric nonlinearity effect with relaxation time of 3 seconds, which is larger than the values reported in the available literature (1 second) [35], to assure complete relief of forming forces. Automatic stabilization was applied to avoid instabilities that cause convergence problems. The initial state of the implicit model was developed from the final state of the explicit spinning model.

Using ABAQUS/Viewer, residual stresses were evaluated in both radial and circumferential (hoop) directions of the spun cup. Springback was evaluated as the radial gap between the spun cup and mandrel. The measurements of thickness

distribution and springback of the experimental spun cup samples have been used for the FE results verification in the subsequent sections. A thickness gauge and a coordinate measuring machine (CMM) were employed in thickness and springback measurements respectively. The internal cup diameter was measured using the CMM and the springback was calculated using the following equation:

$$\text{Springback (mm)} = \frac{\text{Internal Cup Diameter} - \text{Mandrel Diameter}}{2} \quad (3)$$

## B. Results and Discussion

### 1) Validation of FE results

Experimental validation of FE results was carried out using thickness distribution results along the height of two spun cup specimens. Comparison between FE and experimental thickness values was established as shown in Fig. 5. The experimental thickness variation is larger than that of the corresponding FE simulation. This can be attributed to the deeper roller tool penetration in the sheet surface during the experimental runs unlike the finite element runs where less penetration is encountered between mesh nodes. Maximum difference between FE simulation and measured thicknesses is 4.25 % and 6.09 % for specimens (a) and (b) respectively. Thickness variation of the original raw metal sheet may contribute to this difference.

Springback FE results verification was accomplished using the experimental springback values for different thicknesses and coefficients of friction to cover as much as all the processing conditions (Fig. 6). Maximum error in FE results relative to experimental values was found to be 6.30 % and 7.57 % for 2 and 3 mm blank thickness respectively. The difference between FE and experimental results can be attributed to the assumption that coefficient of friction remains constant during all the stages of the spinning process. Additionally, it is difficult to achieve accurate estimate of friction coefficient between roller and metal sheet.

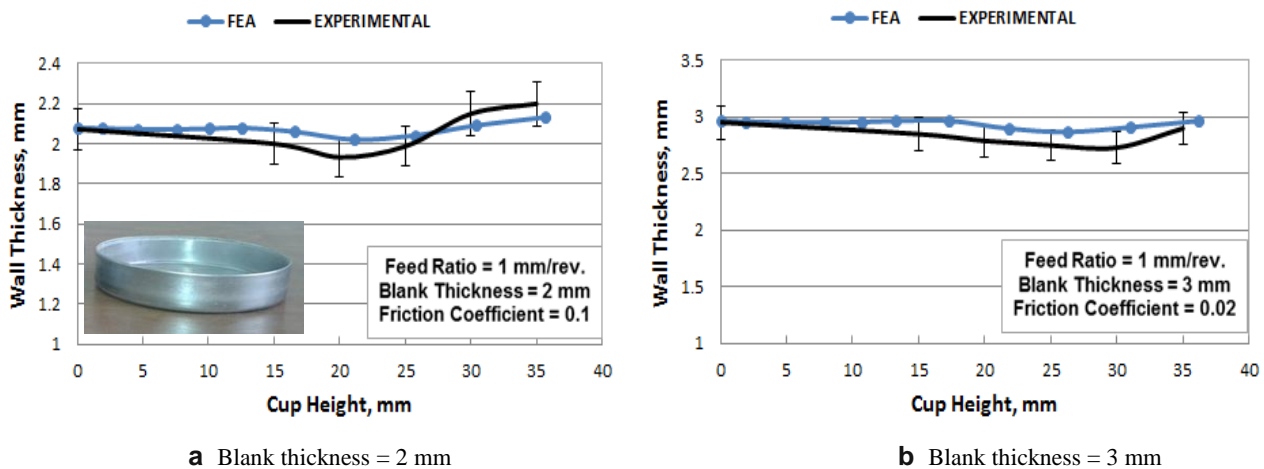


Figure 5. Thickness distribution comparison between FE and experimental results.

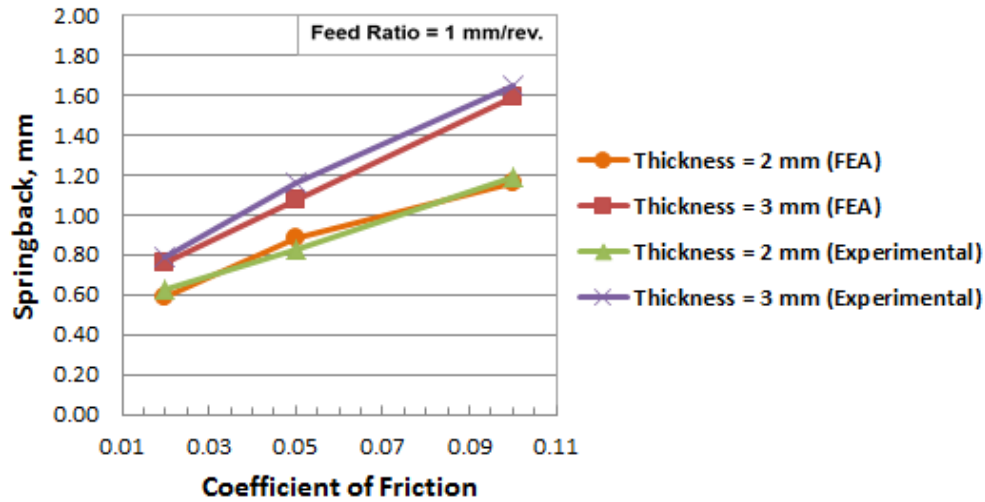


Figure 6. First simulation springback FE and experimental results comparison.

The estimated errors stated above are within the 10 % approved limit [3] so FE results correlate well with the experimental data. As recommended by ABAQUS Analysis User's Guide (2013) [35], energy histories should be used to verify the FE explicit simulation results. Two measures are employed. The first is based on the ratio between the kinetic energy and the internal energy of the deformed sheet which should be within 10% during the majority of the spinning simulation time. This assures that the inertia forces have not significantly affected the results of FE simulation. The second criterion is the ratio between the artificial strain energy to the internal energy which should be maintained below 5 % to guarantee that the problem called hourglassing in the bending action of reduced integration linear elements does not affect the accuracy of the FE analysis. In this study, these energy ratios were observed to be not affected significantly by feed ratio and original sheet thickness but increase as the coefficient of friction increases so the illustrated plot (Fig. 7) is based on the maximum set value of the coefficient of friction (0.1). As shown in the energy ratios plot, the kinetic to

internal energy ratio is obviously high at the start of the spinning process, because the rotation of the blank is dominant with relatively small plastic strain. As the deformation gradually increases, a sharp fall of the ratio takes place. The kinetic energy to internal energy ratio is noticed to be less than 10% for more than 75 % of the process time span, indicating a quasi-static solution, and the artificial strain energy, which results from the artificially hourglass control of the reduced integration linear elements, to internal energy ratio is around 1% during the entire process duration so the dynamic and hourglassing effects are under control.

According to ABAQUS Analysis User's Guide (2013) [35], the implicit FE relaxation analysis results accuracy was checked by comparing the cup metal internal energy with the dissipated static stabilization energy which was found to be very small relative to the internal energy for all simulation runs as in the example shown in Fig. 8. The simulation results are not significantly affected by the static stabilization energy.

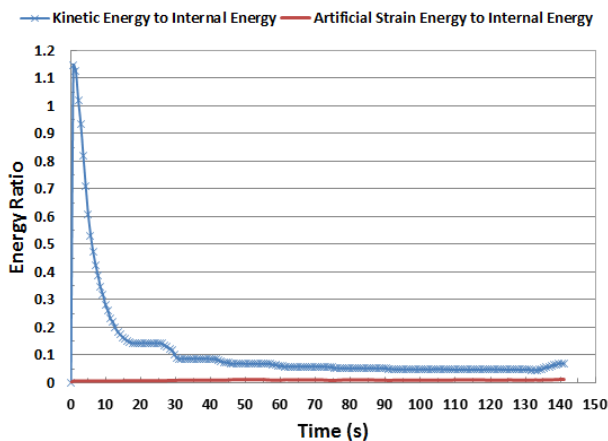


Figure 7. Energy histories in the first FE explicit spinning simulation.

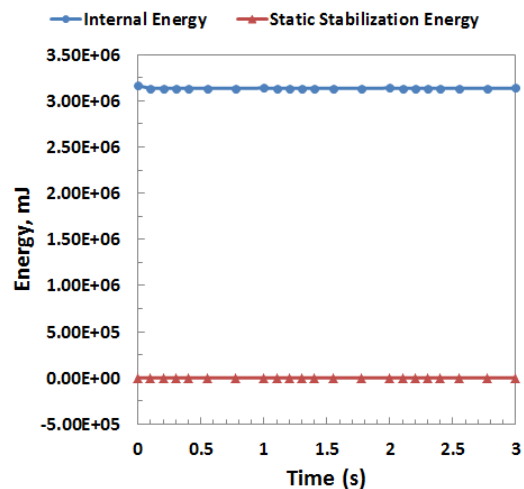


Figure 8. Energy histories during the first FE implicit static relaxation.

## 2) Stages of deformation

FE simulation stages are illustrated in Fig. 9. Von-mises stress is observed to be high in the roller contact region due to the localized plastic deformation. As the sheet rotates away from roller contact, the stress falls down. In the early spinning passes, the roller causes the sheet blank to bend around the mandrel round corner so the axial roller force is relatively high in this stage. During the final spinning pass, the roller compresses the sheet towards the mandrel surface with a large

radial force leading to high induced stresses in the cup wall, as shown in Fig. 9 (d), which cause a springback reaction after releasing the roller away from the cup surface. In the tangential direction of the roller, rolling friction dominates so the tangential roller force is very small with obvious increase at the beginning of the final pass. The spinning forces plot developed from the FE analysis is shown in Fig. 10 for comparison.

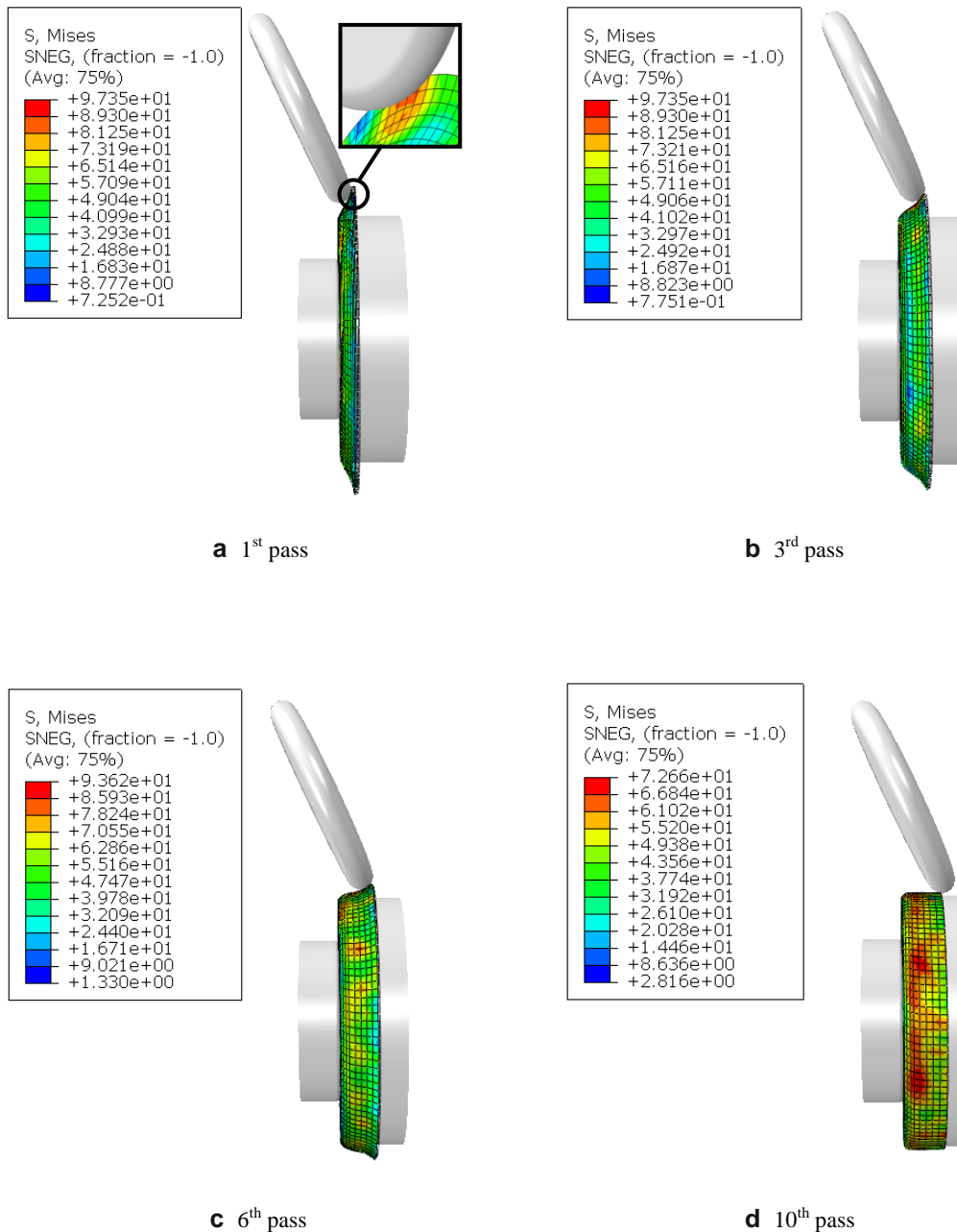


Figure 9. FE simulation stages of deformation in multi-pass spinning.

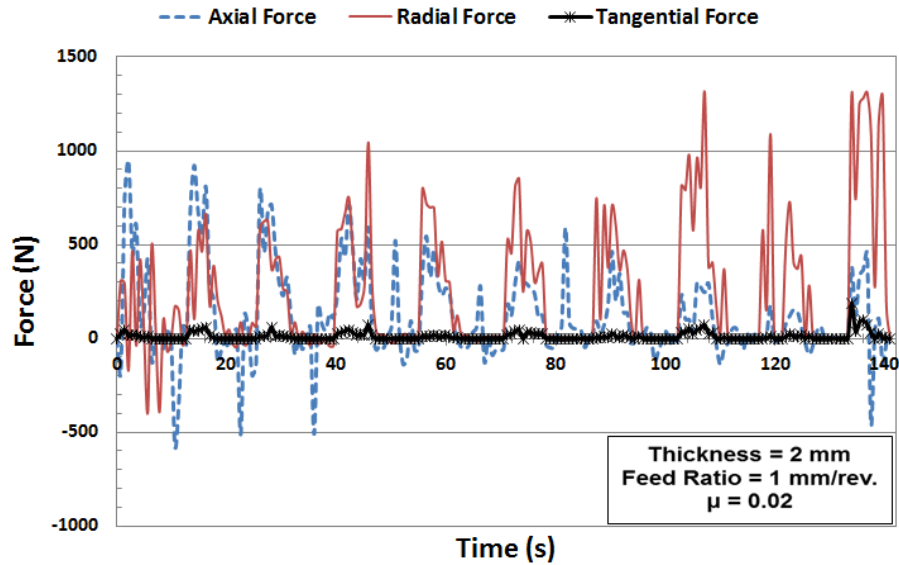


Figure 10. Estimated roller forces distribution against process time using FE analysis.

### 3) Residual Stresses FE results

The residual stress values were obtained according to a local cylindrical coordinate system. The radial stress is defined along the radius of the deformed metal sheet blank, while the tangential (hoop) stress is in the circumferential direction of the cup walls. As the residual stresses are induced in the cup material from the formerly existing *working* stresses during the spinning process especially the final roller pass, the *working* stress fields near the end of the final spinning pass are shown in Fig. 11. At the roller contact zone, the radial *working* stress is highly tensile. As the rotating metal sheet leaves the roller surface the tensile radial *working* stress is recovered to a high compressive state which is then released, after the springback relaxation, to lower compressive radial *residual* stresses spread on the cup wall with severe *tensile* radial residual stress spots at the cup opening as seen in Fig. 12 (a). For the tangential (hoop) *working* stress, highly compressive

values prevail in front of the roller contact point. As the sheet metal is rotated away from the roller contact region, the compressive tangential *working* stress is recovered to high *tensile* stresses around the roller contact region which are obviously decreased to lower tensile values as going further along the cup perimeter away from the roller. These stresses are then released, after the springback relaxation, to fluctuating values of low tensile and low compressive states of stress over the cup wall with high tensile tangential *residual* stress spots at the cup opening as seen in Fig. 12 (b). The high tensile radial and tangential residual stresses spots are highly separated along the perimeter of the cup opening and considered as possible sites of crack initiation during the service life of the spun component especially under high internal pressure on the cup wall. Possible failure locations are mechanical and welded joints where residual stresses can take part.

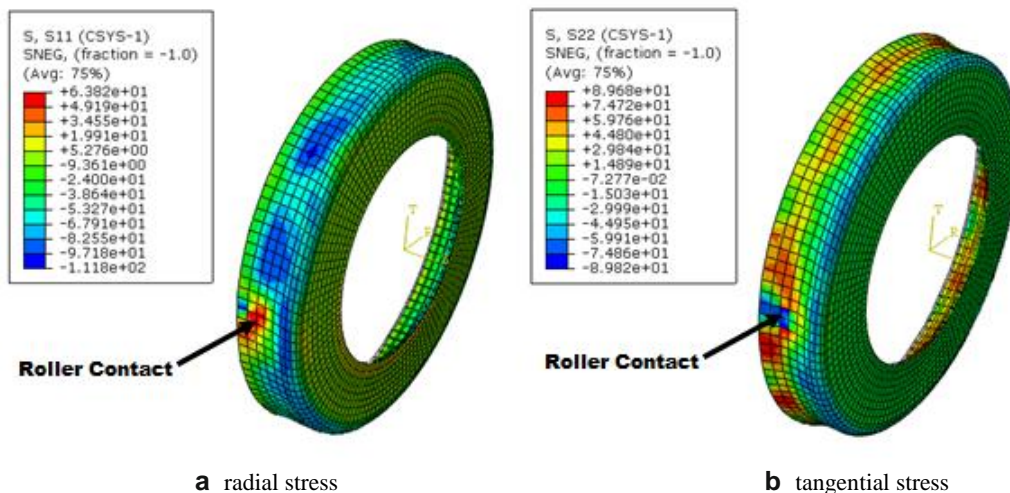


Figure 11. Working stress fields.

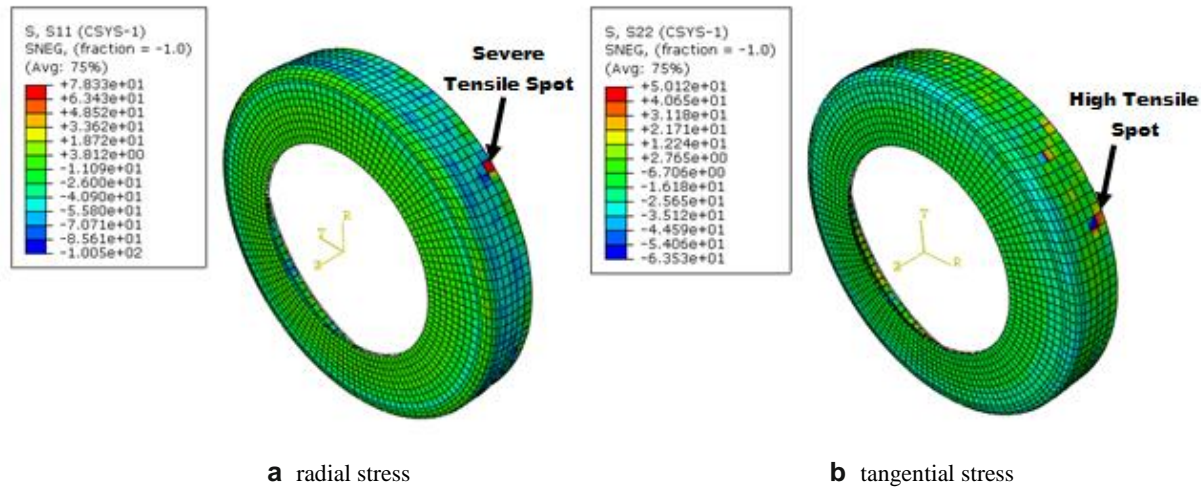


Figure 12. Residual stress fields.

Due to the incremental nature of the spinning process and the localized plastic deformation, the distribution of the resulting residual stresses is fluctuating in both radial and tangential directions as shown in Figs. 13 and 14. Compressive stresses are not critical as they prevent both crack initiation and propagation. High tensile spots are observed at the cup opening separated a distance between 100 and 200 mm along the cup perimeter as shown in Fig. 13. The maximum tensile (most severe) values in radial and tangential directions were considered in the comparison between processing conditions illustrated in Fig. 15. Generally, lower residual stresses in both radial and tangential directions are observed as the sheet thickness increases with small exceptions in the radial direction which can be attributed to uncertainties in the unloading moment due to the in-process localized deformation. Larger sheet thickness is usually associated with high cross sectional area and more stress relief.

As both feed ratio and friction coefficient increase, the radial residual stress decreases, while the tangential residual stress increases. At low feed ratio, the contact area per unit time is small leading to more stress concentration so metal

flow in the radial direction (cup height expansion) is high especially at low friction coefficient which permits the metal to slide freely under the roller. Consequently, the radial residual stress is higher upon unloading. On the other hand, as the feed ratio increases, the rate of reduction in sheet blank diameter is higher leading to higher tangential (hoop) residual stresses upon release of the roller load. This behavior is inflated using higher friction coefficient due to larger forming forces. In most cases, the tangential residual stress is higher than the radial residual stress. This effect is more pronounced as both feed ratio and friction coefficient increase because the rate of cup diameter reduction is higher than the rate of cup height expansion. The exception of this trend is observed at low feed ratio (1 mm/rev.) combined with low friction coefficient (0.02), where the radial residual stress is larger than the tangential residual stress because of larger metal flow rate in the radial direction compared to smaller rate of cup diameter reduction. The two actions are relatively balanced at low feed ratio (1 mm/rev.) combined with intermediate friction coefficient (0.05). As the sheet thickness increases the difference between tangential and radial residual stresses is lower due to smaller rate of loading (higher resistance to deformation).

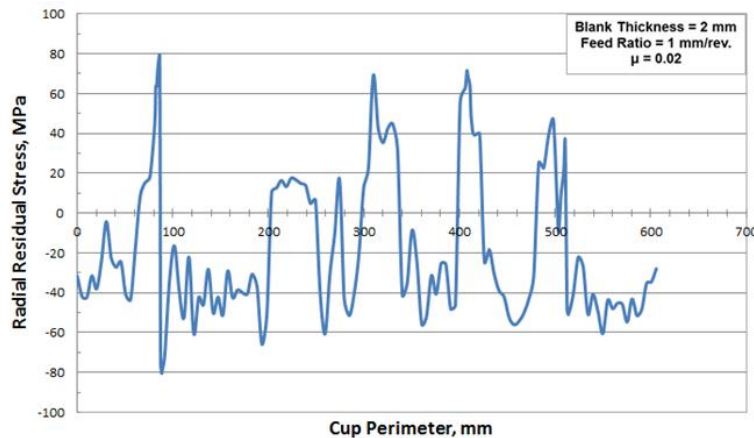


Figure 13. Radial residual stress distribution at cup opening.

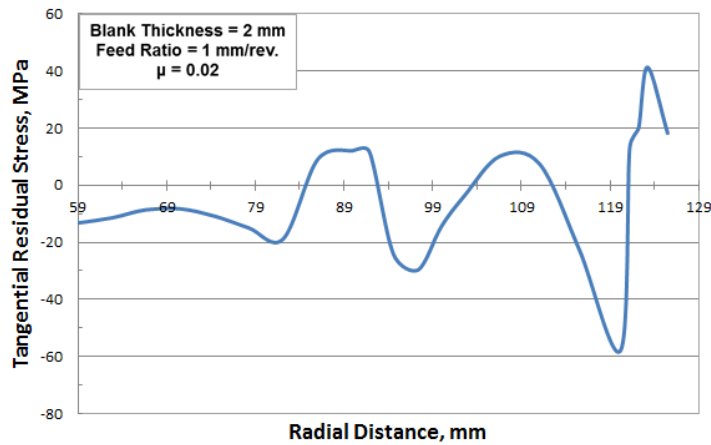


Figure 14. Tangential residual stress distribution.

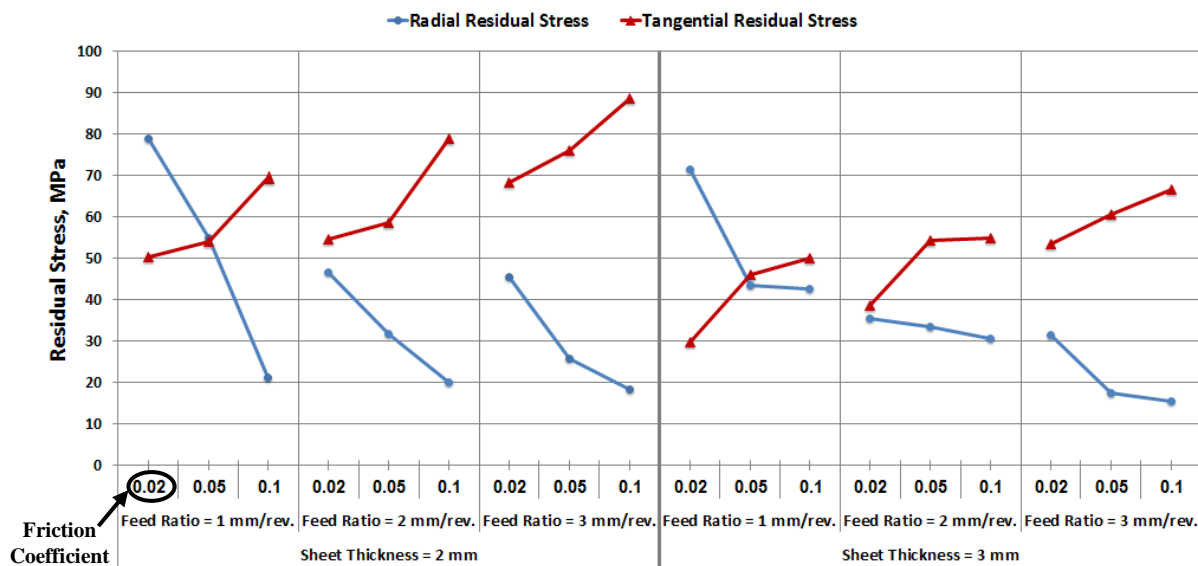


Figure 15. Comparison between radial and tangential residual stresses for all variables combinations.

#### 4) Springback FE results

FE springback results under different processing conditions are illustrated in Fig. 16. An increasing trend is observed with respect to *coefficient of friction*, *feed ratio*, and *sheet thickness*. After each forward pass, the sheet metal has a springback by a certain amount, but the final value of springback in the cup wall is attributed only to the metal behavior in the final pass where there are four controlling parameters that contribute to the springback value; *feed ratio*, *radial force* acting normal to cup wall surface, *friction force* in line with the roller displacement along the cup wall ( $\cong$  radial force  $\times$  friction coefficient), and *unloading moment* which is directly proportional to the sheet thickness cubed [37].

In general, as the loading rate during spinning increases, the elastic recovery of cup wall becomes larger. Comparing figures 16 and 17, it is observed that the springback values are affected by the radial roller force in the final spinning pass. As the feed ratio increases, the radial force increases leading to higher springback reaction in the radial direction of the

mandrel and cup. Also, the feed ratio itself causes further springback due to higher loading rate associated with larger feed ratio as reported by El-Khabeery et al. [15], Kawai et al. [17] and Essa and Hartley [1]. There are some discrepancies between figures 16 and 17; in terms of the effect of both friction coefficient and sheet thickness. This issue can be resolved by considering two further parameters. The first is the friction force which contributes to the loading rate leading to the increasing trend in springback results with higher friction coefficient. The second is the unloading moment which increases with larger sheet thickness resulting in additional springback in the cup wall. As shown in Fig. 16, the rate of rise in springback for the large sheet thickness is higher than that of the small sheet thickness due to larger reactions associated with large thicknesses. The most significant parameter on springback values is friction coefficient followed by sheet thickness.

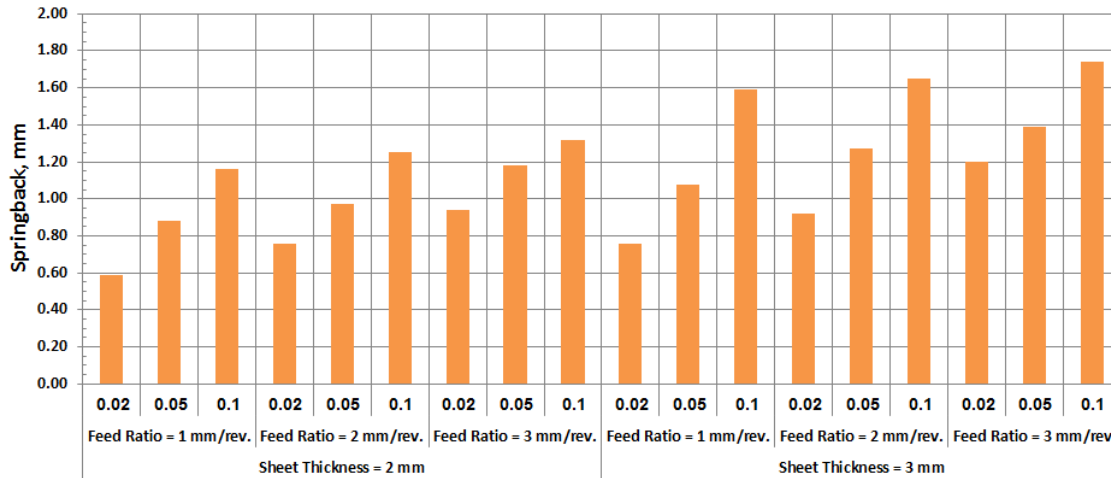


Figure 16. FE springback results under different processing conditions.

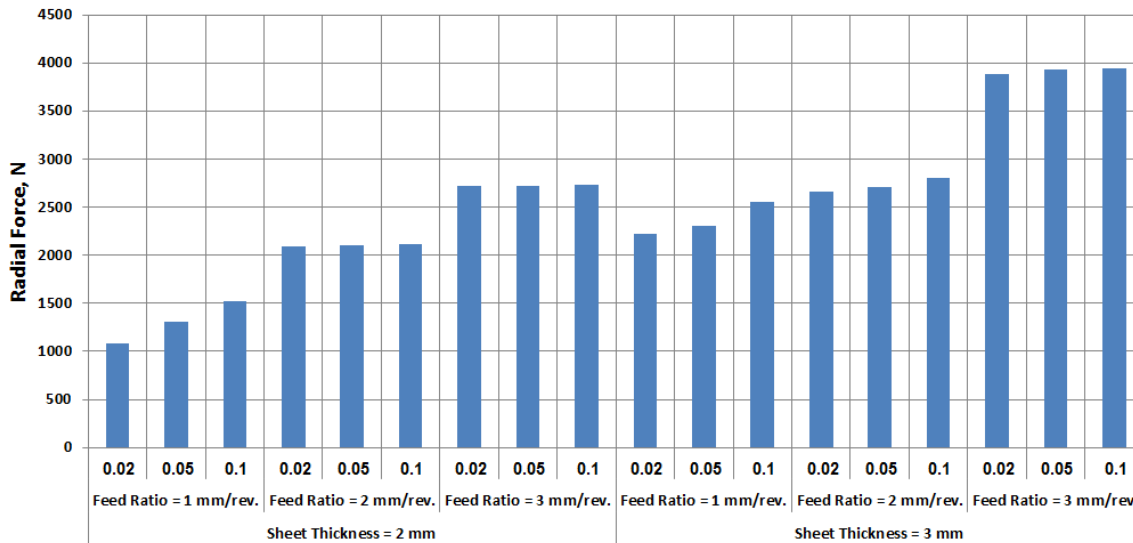


Figure 17. FE radial roller force at the final roller pass under different processing conditions.

## IV. Second Numerical Simulation

### A. Considered Variables

In this set of numerical analyses, it is intended to focus on the effect of number of spinning passes on residual stresses and springback of spun cups. By decreasing the number of passes, the processing time is decreased leading to higher productivity. Three levels of number of passes are employed in this simulation as shown in Table III. The same values of feed ratio in the first simulation are used in the second for the purpose of comparison. Coefficient of friction between the roller and the sheet was set to be 0.02 in all simulation runs because it is associated with both minimum springback and minimum residual stress in the tangential (hoop) direction. The radial residual stress is less critical in pressure vessel

applications. The sheet thickness used is 2 mm for minimum springback. The same FE analysis procedures in the first simulation were applied in the second with nine simulation runs based on all possible variables combinations. There is an overlap between first simulation runs and second simulation runs for number of passes (10), so the actual number of second simulation runs is six. The FE results for thickness distribution and springback were compared with the corresponding experimental CNC spinning results for validation at the same processing parameters.

TABLE III. CONSIDERED VARIABLES IN SECOND NUMERICAL SIMULATION

Variable	Chosen Values		
Number of spinning passes	4	7	10
Feed Ratio (mm/revolution)	1	2	3

## B. Results and Discussion

### 1) Validation of FE results

Using the same procedures employed for the first simulation, the maximum difference in thickness distribution and springback values between FE analysis and experimental runs was determined to validate the second numerical simulation results. As illustrated in Fig. 18, the difference between FE analysis and experimental thickness distributions increases with smaller number of passes due to higher rate of deformation. The maximum error was found to be 5.46%, 4.51%, and 3.67% for number of passes 4, 7, and 10 respectively. The FE springback results go in agreement with

the experimental results with maximum error of 7.36% as shown in Fig.19. The ratio of the kinetic energy to internal energy for the explicit FE simulation was not affected by the number of passes so the energy ratio plot in Fig.20 is developed from 4 passes simulation. This ratio was observed to be below 10% for about 80% of the simulation time. It is also observed that the simulation time was reduced to about the third of its value at 10 passes simulation using the same feed ratio and friction coefficient (Fig.7). The ratio of artificial strain energy to internal energy was found to be around 1%. The static stabilization energy is largely below the internal energy as shown in Fig. 21.

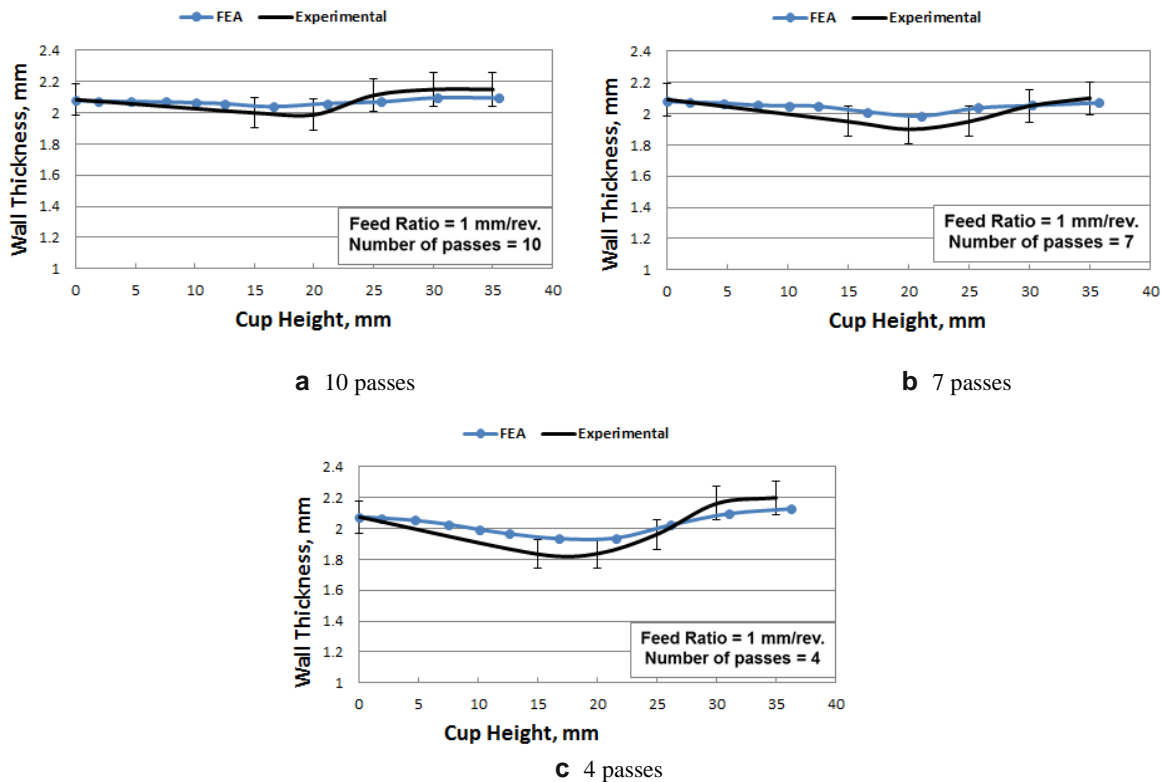


Figure 18. Effect of number of passes on the difference between experimental and FE thickness distribution along spun cup wall.

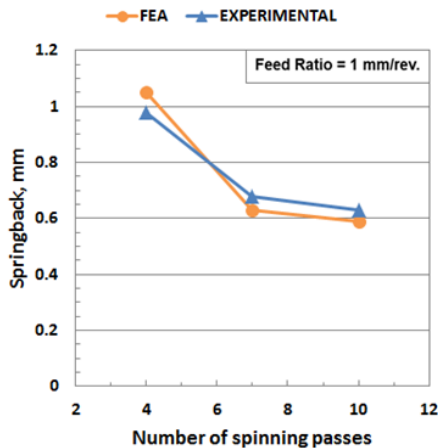


Figure 19. Second simulation springback results validation.

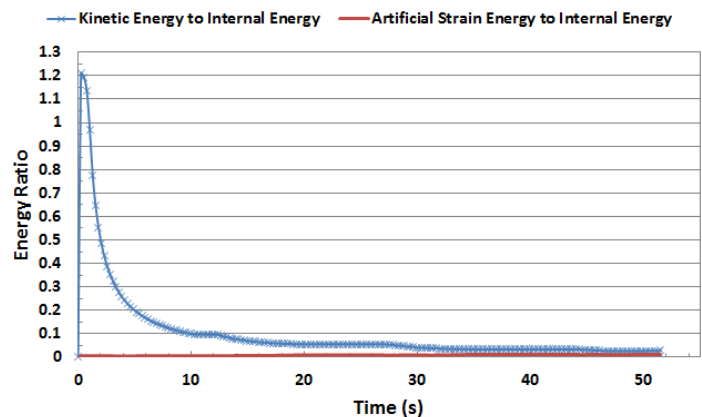


Figure 20. Energy histories in the second FE explicit spinning simulation.

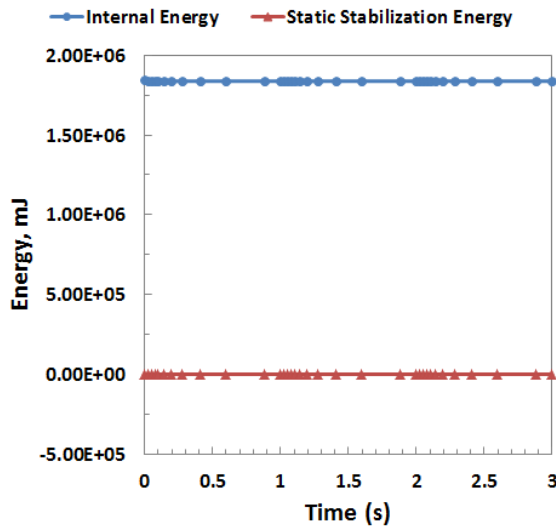


Figure 21. Energy histories during the second FE implicit static relaxation.

### 2) Residual Stresses FE results

Maximum tensile residual stresses were obtained using the same method in the first simulation in both radial and tangential directions. The effect of feed ratio on the trend of both radial and tangential residual stresses is the same as found in the first simulation results. As the feed ratio increases radial residual stress decreases and tangential residual stress increases (Fig. 22). The difference between the both is larger with increasing feed ratio. With larger number of passes, the radial residual stress is increased while the tangential residual stress is decreased. Using small number of passes, the deformation rate per pass is higher with fast reduction of sheet blank diameter inducing higher tangential (hoop) residual stress upon unloading. The larger induced radial residual stresses, as the number of passes increases, can be attributed to more repeated roller contact and indentation along the radial direction of the sheet blank.

In most cases, the difference between tangential and radial residual stresses is greater with small number of spinning passes. An exception exists at feed ratio of 1 mm/rev. using 10 spinning passes where the rate of cup diameter reduction is low leading to smaller value of tangential residual stress relative to the radial residual stress which is inflated due to the stress concentration associated with low feed ratio and more repeated contact. The two residual stresses are nearly balanced at intermediate number of passes (7) using 1 mm/rev. feed ratio.

### 3) Springback FE results

FE springback results with respect to number of spinning passes at different feed ratios are illustrated in Fig. 23. The feed ratio influences the springback values in a trend similar to that observed in the first simulation results. A steady rate of increase in springback is pronounced as the feed ratio increase. Using small number of spinning passes, the loading rate per pass is higher leading to larger unloading reaction with greater value of springback. Similar effect of the number of passes on springback was observed in a recent experimental study by the authors for feed ratios (0.2—1 mm/rev.) [38]. Referring to Fig.18, it is observed that as the cup wall thickness is reduced, the springback value gets larger. This was also found by Wang et al. [20] and can be attributed to the strain hardening effect associated with thickness reduction leading to larger ratio of yield stress  $\sigma_0$  to Young's modulus  $E$  ( $\sigma_0/E$ ). The sheet blank has a springback by a certain amount after each forward pass as shown in Fig. 24. After the first forward pass, the springback is relatively large because only small amount of plastic deformation takes place in the sheet metal especially at the round corner of the mandrel resulting in more elastic recovery. As the process progresses, the plastic deformation increases and the springback value decreases in the subsequent passes. At the final roller pass, the large radial force contributes to further increase in springback value.

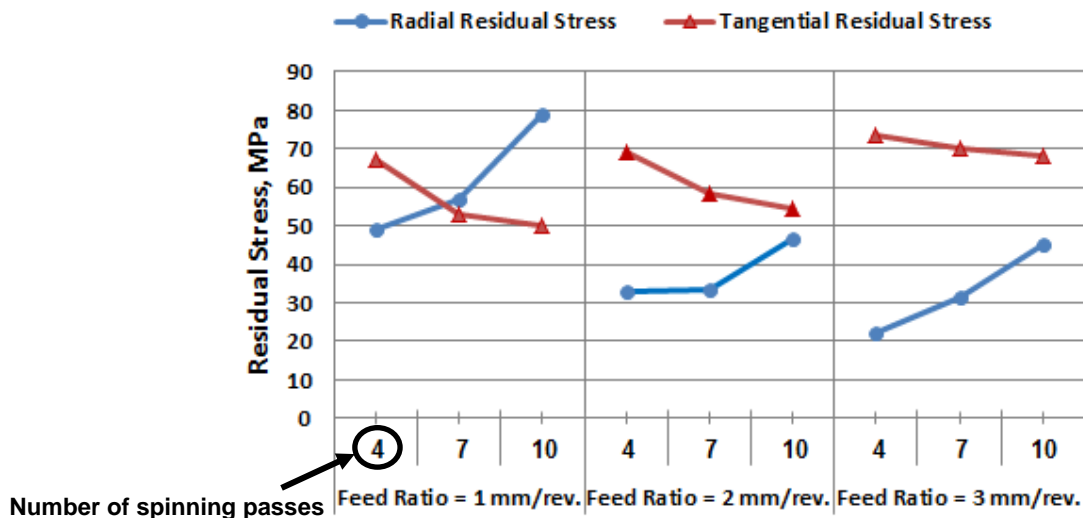


Figure 22. Effect of number of spinning passes at different feed ratios on the residual stresses in radial and tangential directions.

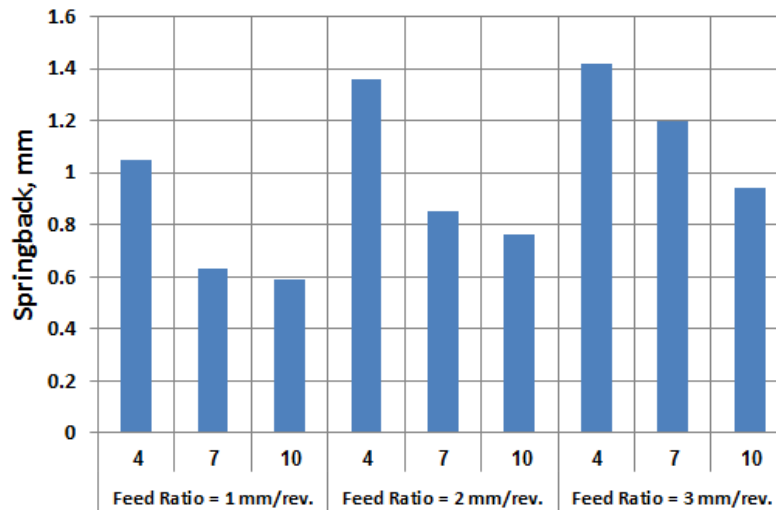


Figure 23. FE springback data variation with number of spinning passes at different feed ratios.

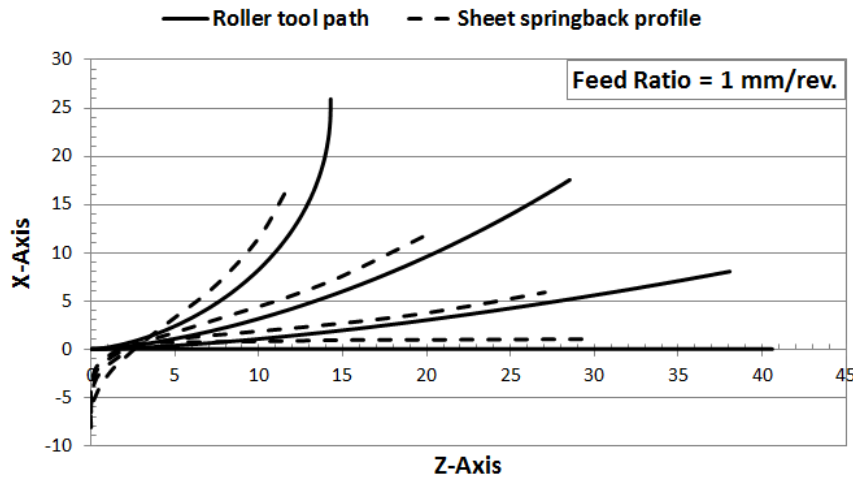


Figure 24. Springback profile of the sheet blank after each forward pass (number of passes = 4).

## v. Conclusions

In this study, two numerical simulations were conducted to predict the residual stresses and springback at different processing conditions in cups produced by multi-pass sheet metal spinning. The following conclusions can be drawn:

- The FE results correlate well with the available experimental data, so confidence in the predicted residual stresses and springback was established.
- The dynamic inertia and hourglassing effects were found to be under control over most of the simulation time.
- The static stabilization energy dissipated during static relaxation of the cups does not affect the accuracy of the FE analysis results.
- The final spinning pass has a major role in the development of springback and residual stresses in the spun cup.
- The residual stresses are fluctuating along the cup wall in both radial and tangential (hoop) directions due to the incremental nature of the process and the localized plastic deformation. Maximum tensile spots are dispersed along the cup opening perimeter.
- The tensile residual stresses particularly in the tangential (hoop) direction are the controlling parameter of crack initiation and propagation during the service life of spun components especially those used in high-pressure vessels. No problem is encountered with the presence of compressive residual stresses in all directions.

- Mostly, the tangential (hoop) residual stresses are more serious on the performance of spun cups than the radial residual stresses.
- Minimum tangential (hoop) residual stresses for safe tank bottoms can be achieved using higher sheet thickness, minimum feed ratio, small coefficient of friction and large number of spinning passes.
- Minimum radial residual stresses are established with larger sheet thickness, maximum feed ratio, high friction coefficient, and small number of spinning passes.
- Minimum springback values for accurate aerospace and industrial components are obtained using smaller sheet thickness, minimum feed ratio, low coefficient of friction, and large number of passes.
- Optimum combination between small springback and safe spun component can be realized using low levels of feed ratio and friction coefficient with large number of spinning passes.
- There appears to be some dependence of springback values on wall thickness reduction of the spun cups, which can be attributed to strain hardening effect associated with thickness reduction and leading to higher yield stress  $\sigma_0$  to Young's modulus E ratio ( $\sigma_0/E$ ).

### Acknowledgment

The authors gratefully acknowledge the appreciated support from all staff members at LORD INTERNATIONAL Co., EGYPTIAN COPPER WORKS and AL -EZZ - DEKHEILA STEEL Co.

### References

- [1] K. Essa, and P. Hartley, "Optimization of conventional spinning process parameters by means of numerical simulation and statistical analysis," Proceedings of the Institution of Mechanical Engineers, Part B: Journal of Engineering Manufacture, vol. 224, pp. 1691-1705, 2010.
- [2] K. Essa, "Finite element prediction of deformation mechanics in incremental forming processes," Ph.D. thesis, University of Birmingham, UK, 2011.
- [3] L. Wang, "Analysis of material deformation and wrinkling failure in conventional metal spinning process," Ph.D. thesis, Durham University, UK, 2012.
- [4] F. Klocke, "Manufacturing Processes 4; Forming," Springer, 2013.
- [5] O. Music, J.M. Allwood, and K. Kawai, "A review of the mechanics of metal spinning," Journal of Materials Processing Technology, vol. 210(1), pp. 3-23, 2010.
- [6] G. Shen, N. Cooper, N. Ottow, R. Goetz, and J. Matlik, "Integration and automation of residual stress and service stress modeling for superalloy component design," Superalloys 2012 - Proceedings of the 12th International Symposium on Superalloys, Seven Springs, PA, United states, pp. 129-134, 2012.
- [7] M. Watson, and H. Long, "Wrinkling failure mechanics in metal spinning," Procedia Engineering, vol. 81, pp. 2391 - 2396, 2014.
- [8] H. Zoghi, A.F. Arezoodar, and M. Sayeafabi, "Effect of feed and roller contact start point on strain and residual stress distribution in dome forming of steel tube by spinning at an elevated temperature,"

Proceedings of the Institution of Mechanical Engineers Part B: Journal of Engineering Manufacture, vol. 226(11), pp. 1880-1890, 2012.

- [9] C.H. Gür, and E.B. Arda, "Effect of tube spinning and subsequent heat treatments on strength, microstructure and residual stress state of AISI/SAE type 4140 steel," Materials Science and Technology, vol. 19(11), pp. 1590-1594, 2003.
- [10] Z. Zhang, and G.-Y. Su, "Measuring method of z- $\theta$  directional residual shear stress in spun thin-walled tube," Material Science and Technology, vol. 19(5), pp. 111-115, 2011.
- [11] F. Hua, Y. Yang, D. Guo, W. Tong, and Z. Hu, "Elasto-plastic FEM analysis of residual stress in spun tube," Journal of Materials Science and Technology, vol. 20(4), pp. 379-382, 2004.
- [12] Y. Li, Z.-C. Xu, Y. Tang, and Z.-X. Zeng, "Numerical simulation of high-speed spinning of thin-wall copper tube with axial micro-grooves," Journal of South China University of Technology (Natural Science), vol. 38(1), pp. 128-133, 2010.
- [13] D. Marini, D. Cunningham, and J. Corney, "A review of flow forming processes and mechanisms," Key Engineering Materials, vol. 651-653, pp. 750-758, 2015.
- [14] P. Šugár, J. Šugárová, and J. Petrovič, "Surface integrity of metal spun parts," Key Engineering Materials, vol. 581, pp. 391-396, 2014.
- [15] M.M. EL-Khabeery, M. Fattouh, M.N. EL-Sheikh, and O.A. Hamed, "On the conventional simple spinning of cylindrical aluminium cups," International Journal of Machine Tools and Manufacture, vol. 31 (2), pp. 203-219, 1991.
- [16] L. Wang, and H. Long, "Investigation of material deformation in multi-pass conventional metal spinning," Materials and Design, vol. 32, pp. 2891-2899, 2011.
- [17] K. Kawai, L.-N. Yang, and H. Kudo, "A flexible shear spinning of axisymmetrical shells with a general-purpose mandrel," Journal of Materials Processing Technology, vol. 192-193, pp. 13-17, 2007.
- [18] G. Venkateshwarlu, K.R. Kumar, T.A.J. Reddy, and G. Gopi, "Experimental investigation on spinning of aluminum alloy 19500 cup," International Journal of Engineering Science and Innovative Technology (IJESIT), vol. 2(1), pp. 357-363, 2013.
- [19] D. Han, M. Zhan, and H. Yang, "Deformation mechanism of TA15 shells in hot shear spinning under various load conditions," Rare Metal Materials and Engineering, vol. 42(2), pp. 243-248, 2013.
- [20] Y.-J. Wang, G. Fang, J.-H. Zhang, P. Zeng, X.-G. Zhang, and G. Shi, "Finite element simulation for the spinning process of an automobile spokes with varying thickness," Material Science and Technology, vol. 20(3), pp. 103-108, 2012.
- [21] Q. Xia, S. Shima, H. Kotera, and D. Yasuhuku, "A study of the one-path deep drawing spinning of cups," Journal of Materials Processing Technology, vol. 159 (3), pp. 397-400, 2005.
- [22] M. Jurković, Z. Jurković, and M. Mahmić, "An analysis and modelling of spinning process without wall-thickness reduction," METALURGIJA, vol. 45 (4), pp. 307-312, 2006.
- [23] B. Rentsch, N. Manopulo, and P. Hora, "Numerical modelling, validation and analysis of multi-pass sheet metal spinning processes," International Journal of Material Forming, vol. 10(4), pp. 641-651, 2017.
- [24] Q. Kong, Z. Yu, Y. Zhao, H. Wang, and Z. Lin, "Theoretical prediction of flange wrinkling in first-pass conventional spinning of hemispherical part," Journal of Materials Processing Technology, vol. 246, pp. 56-68, 2017.
- [25] Q. Kong, Z. Yu, Y. Zhao, H. Wang, and Z. Lin, "A study of severe flange wrinkling in first-pass conventional spinning of hemispherical part," The International Journal of Advanced Manufacturing Technology, vol. 91, pp. 1-16, 2017.
- [26] T. Gan, Z. Yu, Y. Zhao, S.A. Evsyukov, and X. Lai, "Effects of backward path parameters on formability in conventional spinning of aluminum hemispherical parts," Transactions of Nonferrous Metals Society of China, vol. 28(2), pp. 328-339, 2018.
- [27] M. Zhan, Q. Zhou, H. Yang, and J. Zhang, "Establishment of 3D FEM model of multi-pass spinning," Chinese Journal of Mechanical Engineering, vol. 20(4), pp. 19-23, 2007.

- [28] M. Zhan, H. Yang, J.H. Zhang, Y.L. Xu, and F. Ma, "3D FEM analysis of influence of roller feed rate on forming force and quality of cone spinning," *Journal of Materials Processing Technology*, vol. 187–188, pp. 486–491, 2007.
- [29] Q. Bai, H. Yang, and M. Zhan, "Finite element modeling of power spinning of thin-walled shell with hoop inner rib," *Transactions of Nonferrous Metals Society of China*, vol. 18(1), pp. 6–13, 2008.
- [30] L. Wang, H. Long, D. Ashley, M. Roberts, and P. White, "Effects of the roller feed ratio on wrinkling failure in conventional spinning of a cylindrical cup," *Proceedings of the Institution of Mechanical Engineers, Part B: Journal of Engineering Manufacture*, vol. 225 (11), pp. 1991 – 2006, 2011.
- [31] L. Wang, and H. Long, "A study of effects of roller path profiles on tool forces and part wall thickness variation in conventional metal spinning," *Journal of Materials Processing Technology*, vol. 211, pp. 2140– 2151, 2011.
- [32] B. Awiszus, and S. Härtel, "Numerical simulation of non-circular spinning: a rotationally non-symmetric spinning process," *Production Engineering Research and Development*, vol. 5(6), pp. 605-612, 2011.
- [33] C.-H. Liu, "The simulation of the multi-pass and die-less spinning process," *Journal of Materials Processing Technology*, vol. 192–193, pp. 518–524, 2007.
- [34] K. Essa, and P. Hartley, "Numerical simulation of single and dual pass conventional spinning processes," *International Journal of Material Forming*, vol. 2, pp. 271–281, 2009.
- [35] ABAQUS analysis user's Guide, ver. 6.13, 2013.
- [36] T. Sangkharat, and S. Dechjarearn, "Spinning process design using finite element analysis and taguchi method," *Procedia Engineering*, vol. 207, pp. 1713–1718, 2017.
- [37] W.F. Hosford, and R.M. Caddell, "Metal Forming Mechanics and Metallurgy," Third Edition, Cambridge University Press, New York, 2007.
- [38] M. Abd-Alrazzaq, M. Ahmed, and M. Younes, "Experimental Investigation on the Geometrical accuracy of the CNC multi-pass sheet metal spinning process," *Journal of Manufacturing and Materials Processing*, vol. 2, 59, 2018.

About Author (s):



**Mohammad A. Younes, Professor**  
*Department of Production Engineering,  
Faculty of Engineering, Alexandria University,  
Egypt.*